

Creation and manipulation of Schrödinger cat states based on semiclassical predictions

N. G. Veselkova,¹ R. Goncharov,^{2,3,*} and Alexei D. Kiselev^{4,3,2,†}

¹*Saint-Petersburg State Institute of Technology, 26, Moskovski ave., St. Petersburg, 190013, Russia*

²*Quantum Information Laboratory, ITMO University, Kadetskaya Line, 3, St. Petersburg, 199034, Russia*

³*Leading Research Center "National Center for Quantum Internet",
ITMO University, Birzhevaya Line, 16, St. Petersburg, 199034, Russia*

⁴*Laboratory of Quantum Processes and Measurements,
ITMO University, 199034 Kadetskaya Line 3b, Saint Petersburg, Russia*

(Dated: January 17, 2025)

We consider the generation of Schrödinger cat states using a quantum measurement-induced logical gate where entanglement between the input state of the target oscillator and the Fock state of the ancillary system produced by the quantum non-demolition entangling C_Z operation is combined with the homodyne measurement. We utilize the semiclassical approach to construct both the input-output mapping of the field variables in the phase space and the wave function of the output state. This approach is found to predict that the state at the gate output is represented by a minimum disturbed cat-like state which is a superposition of two initial state copies symmetrically displaced by momentum variable. For the target oscillator prepared in the coherent state, we show that the fidelity between the exact solution for the gate output state and the “perfect” Schrödinger cat reconstructed from the semiclassical theory can reach high values exceeding 0.99.

I. INTRODUCTION

Continuous-variable (CV) optical systems are a promising platform for large-scale quantum information processing. The properties of the CV schemes with embedded non-Gaussian gates are being actively investigated nowadays [1–3]. Along with the large-scale Gaussian operations enabled by the cluster states [4, 5], quantum non-Gaussian gates are essential components [6, 7] for a variety of practical tasks in optical quantum technology and advanced quantum information processing including quantum communication, quantum computation, quantum algorithms, and quantum control. It has been found that non-Gaussianity [8–11] in the form of non-Gaussian quantum states [12–21] and non-Gaussian operations [2, 22–27] is crucial, due to the limited capability of Gaussian states and operations, for various CV quantum information protocols required for quantum teleportation [28–30], entanglement distillation [31, 32], error correction [33, 34], fault-tolerant universal quantum computing [2, 35–38], loophole-free test of quantum non-locality [39, 40], and quantum simulations [41, 42].

Optical Schrödinger cat states have been considered as a substantial non-Gaussian resource for practical employment in quantum science since the early 2000s [43, 44]. They play a considerable role in up-to-date quantum technologies [44–55] and CV quantum information processing [44, 54, 56, 57], including quantum metrology [52, 58–60], quantum teleportation [61, 62], quantum communication and quantum repeaters [48–51], and error correction schemes for fault-tolerant quantum computing [43, 45, 46, 63–67]. From a basic research point of view, the Schrödinger cat states have been of great interest both for testing the foundations of quantum mechanics and determining the limits of its validity by exploring the quantum-to-classical transition.

The main challenge for most applications in quantum information technologies is to produce Schrödinger cat-like states whose “size”, namely the distance in phase space between the two coherent states, is sufficiently large to enable good-quality operations [43, 45, 68–70]. Such large-amplitude coherent-state superpositions exhibiting unique non-classical attributes such as sub-Planck phase-space structures [71] and non-Gaussian interference features [72–74] are commonly used as a base for preparing qubits in CV quantum computing [43, 75], and a resource for quantum error-correcting codes [35, 76–78].

Currently, cat-like quantum superpositions are being successfully simulated in various physical systems [79–83], but developing realistic schemes to produce optical Schrödinger cat states with a large number of photons and controlled quantum properties remains a challenging task. To achieve this goal, a variety of well-established conditional generation approaches have been proposed, including schemes based on such non-Gaussian operations as photon-number measurement and subtraction [47, 84–90] and other cat-states generation methods [12, 69, 70, 86, 91–93], some of which have been successfully implemented [57, 69, 88, 89, 91–93]. In nondeterministic schemes which create the target state only under predetermined conditions, the auxiliary channel can be prepared in the Fock state [68, 69, 91, 93, 94], or even in complex superpositions which arise in the iterative cat breeding schemes [69, 70, 95, 96]. In particular, a low-frequency regime of optical Schrödinger cat state generation using the Fock state as a resource, a beam splitter as an entangling element, and homodyne detection was experimentally demonstrated [69, 91].

In this paper, we consider the conditional generation of a Schrödinger cat state from an arbitrary coherent state employing a two-node non-Gaussian gate (“cat gate”) based on the Fock state of the ancillary oscillator as an elementary non-Gaussian resource, the quantum non-demolition (QND) entangling operation C_Z , and the projecting homodyne measurement. We show that a CV quantum circuit with such measurement-induced two-node non-Gaussian element may generate a cat-

* Email address: rkgoncharov@itmo.ru

† Email address: alexei.d.kiselev@gmail.com

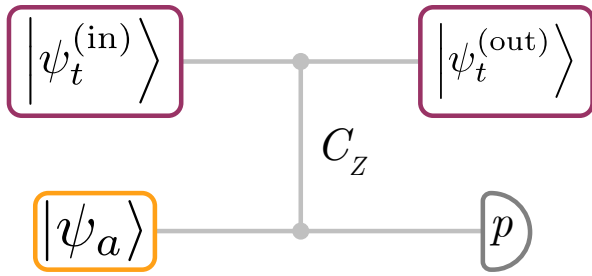


Figure 1. The scheme for conditional generation of cat states employing a two-node non-Gaussian gate (“cat gate”) using an ancilla oscillator in the photon number (Fock) state. The states $|\psi_t^{(\text{in})}\rangle$ and $|\psi_a\rangle$ of the target and ancillary oscillators are sent to the input of the gate. After applying the entangling non-demolition C_Z operation, a homodyne measurement of the ancilla momentum is performed. Depending on the measurement outcome y_m , the state of the composite system collapses to a cat-like superposition state $|\psi_t^{(\text{out})}\rangle$.

like quantum superposition and, under optimal conditions, the output state is close to the “perfect” Schrödinger cat state which is a superposition of the two (in general, more) symmetrically displaced undistorted copies of the input state. In parallel with the exact theoretical description of the gate operation, we introduce a clear visual interpretation of the output state based on the semiclassical mapping of the input field variables and construct the semiclassical wave function of the undisturbed cat state closest to the exact output state.

The scheme can produce optical Schrödinger cat states of any desired size with high fidelity exceeding 0.99 and we find the conditions under which the gate generates high-quality cat-like states by computing the fidelity between the exact output state and the superposition of two symmetrically displaced undistorted copies of the input coherent state. We also demonstrate the output state quantum statistics in terms of the Wigner function.

The paper is organized as follows. In Section II, we provide a semiclassical description of the creation of Schrödinger cat states using a measurement-induced two-node non-Gaussian logic gate. In Section III, we derive the target oscillator’s exact output state following the non-Gaussian gate’s action, providing an analytic expression for the output wave function. Section IV focuses on generating cat-like states from a coherent state. Section V concludes the paper. Technical details on the method used to evaluate the Wigner functions are relegated to Appendix A.

II. SEMICLASSICAL DESCRIPTION OF SCHRÖDINGER CAT STATE CREATION

Following to Ref. [97], we consider the measurement-induced two-node non-Gaussian logic gate shown in Fig. 1. It can be seen that this gate uses the photon number (Fock) state of the ancilla as an elementary non-Gaussian resource, the C_Z operation which entangles an input signal with the ancilla, and the projecting homodyne measurement. An essential feature of the scheme is that the ancilla measurement outcome

provides multivalued information about the target oscillator output momentum that gives rise to a cat-like output state. This peculiarity can be easily interpreted [98] in terms of a clear visual representation of the quadrature amplitudes transformations in the scheme which demonstrates that two-component (or multi-component) Schrödinger cat state arises when the measurement outcome is compatible with not one but with multiple (two or more) values of the target oscillator variables. Such a pictorial description might also be useful for the analysis of measurement-induced schemes based on more complicated non-Gaussian resource states where a closed-form (analytic) expression for the output state is not available.

According to Ref. [97], for the photon number state-based gate, a cat-like superposition of two “copies” of the target state closest to the exact output state can be effectively evaluated using the semiclassical approximation. To this end, we assume the Heisenberg representation and consider how the canonical variables, coordinate and momentum operators, of both oscillators are transformed under the action of the entangling operation. Then the relations imposed on the canonical variables are treated as c-numerical and the measurement of the ancilla momentum is also described semiclassically by substituting momentum with its observed value giving an explicit expression for the input-output mapping between the target oscillator variables.

More specifically, let us introduce the coordinate q and momentum p operators for each of the oscillators in conventional way as $a = (q + ip)/\sqrt{2}$, where $[q, p] = i$. Next, the two-mode entangling unitary evolution operator $C_Z = \exp(iq_1q_2)$ is applied to the initial state of the oscillators. In the Heisenberg picture, we have the relation

$$\begin{aligned} q^{(\text{out})} &= q^{(\text{in})}, & p^{(\text{out})} &= p^{(\text{in})} + q_a^{(\text{in})}, \\ q_a^{(\text{out})} &= q_a^{(\text{in})}, & p_a^{(\text{out})} &= p_a^{(\text{in})} + q^{(\text{in})}, \end{aligned} \quad (1)$$

where the index a marks the ancilla variables. In what follows, the variables of the subsystems that enter Eq. (1) will be interpreted as c-numbers. For an ancilla initially prepared in the Fock resource state $|n\rangle$, n is the photon number, the semiclassical amplitudes q_a and p_a are related as follows

$$q_a^{(\text{in})2} + p_a^{(\text{in})2} = 2n + 1. \quad (2)$$

After applying the operation C_Z , the resource state is described by the *resource curve equation*

$$q_a^{(\text{out})2} + (p_a^{(\text{out})} - q^{(\text{in})})^2 = 2n + 1, \quad (3)$$

which is a circle of radius $\sqrt{2n + 1}$ vertically displaced by $q^{(\text{in})}$ (see Fig. 2).

Finally, a homodyne measurement of the ancillary oscillator momentum $p_a^{(\text{out})}$ with outcome y_m is described by the change $p_a^{(\text{out})} \rightarrow y_m$ giving two values of the ancilla coordinate: $q_a^{(\text{out})} = x_a^{(\pm)} \equiv \pm\sqrt{2n + 1 - (y_m - q^{(\text{in})})^2}$. As is shown in Fig. 2, these values are the coordinates of the points of intersection of the horizontal line $p_a^{(\text{out})} = y_m$ with the circle (3). Figure 2 presents a clear geometrical description based on the semiclassical mapping that directly indicates the

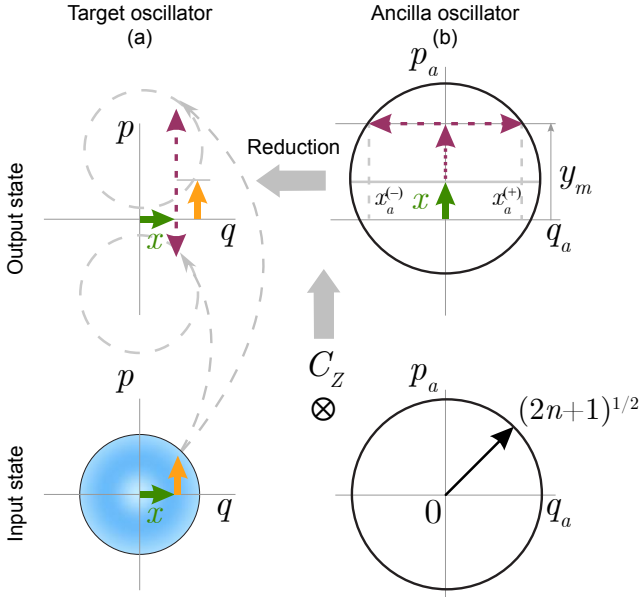


Figure 2. The measurement-induced semiclassical mapping of the quadrature amplitudes (canonical variables) of the target q, p [(a) column] and ancilla q_a, p_a [(b) column] oscillators performed by the gate is schematically shown here. The initial canonical variables approximated by c-numbers are randomly chosen in phase space within the support region (in the picture it is a circle in the vicinity of the origin) [the bottom row of (a) column] of the target oscillator field, and represented by the arrows; where the ancilla is initially prepared in the Fock state with the number of photons n represented by a circle of radius $\sqrt{2n+1}$ in phase space [the bottom row of (b) column]. At first, the randomly chosen initial amplitudes undergo the entangling non-demolition C_Z operation. Then a homodyne measurement of the ancilla momentum with the outcome y_m is performed [the top row of (b) column], which ensures measurement-induced splitting of the ancilla coordinate (as marked by horizontal dashed arrows) resulting in the displacement of the copies along the momentum axis in the output state due to entanglement. As a result, the state of the composite system collapses to the two-component cat-like superposition state, the components of which are symmetrically displaced in phase space along the momentum axis by $x_a^{(\pm)} = \pm\sqrt{2n+1 - (y_m - x)^2}$, where x is the initial coordinate of the target oscillator [the top row of (a) column].

number, position, and offset of these points depending on the target oscillator coordinate.

Owing the quantum correlation of the target and ancillary subsystems, the ambiguity of the solution for the ancilla coordinate arising from results in the multivaluedness of the target oscillator momentum (hereafter $x \equiv q$ denotes the target oscillator coordinate) that enter the semiclassical mapping

$$(q^{(\text{out})}, p^{(\text{out})}) = (x, p^{(\text{in})} \pm \sqrt{2n+1 - (y_m - x)^2}), \quad (4)$$

and, under additional conditions discussed below, to the emergence of a cat-like state which is a quantum superposition of two macroscopically distinguishable coherent states.

Note that Eq. (4) implies distortion of the copies of the initial state: at any fixed y_m the region of phase space where $x \approx y_m$ experiences the greatest displacement that decreases with the

magnitude of the difference $|y_m - x|$ leading to deformation of the cat components. The distortion of copies is minimal if, for a given measurement outcome y_m , the resource curve at its intersection points is $x_a^{(\pm)}$ of the horizontal line $p_a^{(\text{out})} = y_m$ is close to vertical (Fig. 2, the top row of (b) column). In this case, measurement-induced splitting of the ancilla coordinate (indicated by dashed horizontal arrows) is almost independent of the target oscillator coordinate x (i.e., from the resource curve's vertical shift). In general, the ideal case is when the coordinates of the intersection points $x_a^{(\pm)}$ do not change when shifting the position x of the initial point, chosen within the support region of the target oscillator in the phase space. For the resource Fock state, as can be seen from Fig. 2, the deformation of the copies is minimal for the phase space points belonging to the region $x \approx y_m$ —for them the horizontal dashed arrows lie on the diameter of the Fock circle.

In order to illustrate these effects, let us assume that the target oscillator is prepared in the coherent state $|\alpha\rangle$ with the amplitude $\alpha = (x_0 + ip_0)/\sqrt{2}$ and the uncertainty region $(x - x_0)^2 + (p - p_0)^2 \leq 1$ indicated in Fig. 3 as a magenta colored circle. Figure 3 shows what happens to the uncertainty circle under the semiclassical mapping $(x, p) \mapsto (x, p \pm \sqrt{2n+1 - (y_m - x)^2})$ (images of the circle are shown as the orange colored regions) at different values of y_m . In Fig. 3 the area liable to minimal deformation is: (a) $x \approx 3$ (the center of the uncertainty circle); (b) $x \approx 2$ (the left edge of the uncertainty circle); (c) $x \approx 1$ (the set of points outside the uncertainty region of the initial coherent state).

The obtained semiclassical relations can be used to reconstruct the target oscillator wave function when the ancilla oscillator in the Fock state. Indeed, in the semiclassical treatment, as is shown in [97], the input-output mapping performed by the gate under consideration

$$\psi_{\text{out}}(x) = \psi_{\text{in}}(x)\varphi_{\text{scl}}(x), \quad (5)$$

can be described by multiplying the input wave function of the target oscillator $\psi_{\text{in}}(x)$ by the factor

$$\begin{aligned} \varphi_{\text{scl}}(x) \sim & \sqrt{P^{(+)}(x, y_m)} \exp\left[i \int dx \delta p(x)\right] \\ & + \sqrt{P^{(-)}(x, y_m)} \exp\left[-i \int dx \delta p(x)\right], \end{aligned} \quad (6)$$

which is the sum of the added factors coming from two intersection points of the resource curve with the horizontal line $p_a^{(\text{out})} = y_m$. It depends only on the state of the ancilla, the target oscillator coordinate x , and the ancilla momentum measurement outcome y_m . Formula (5) reflects universality of the gate implying that its action is independent of the target oscillator state at the input of the scheme.

From Eq. (4), we have

$$\delta p(x) \equiv p^{(\text{out})} - p^{(\text{in})} = \pm \sqrt{2n+1 - (y_m - x)^2} \quad (7)$$

and, according to [97], the quantities $P^{(\pm)}$ given by

$$P^{(+)}(x, y_m) = P^{(-)}(x, y_m) \sim \frac{1}{|\delta p(x)|} \quad (8)$$

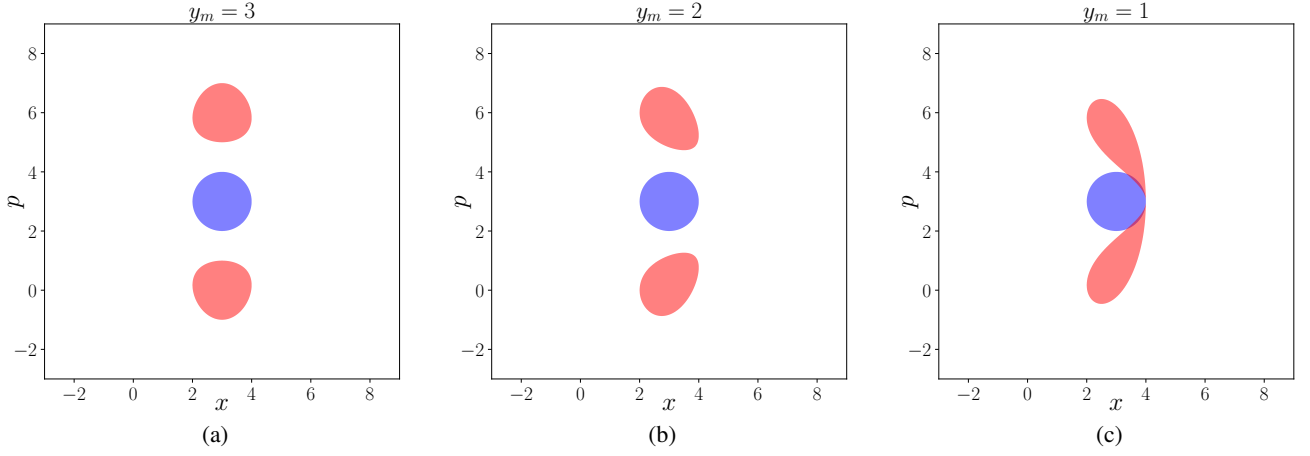


Figure 3. Semiclassical mapping of quadrature amplitudes (see Eq. (4)) for the target oscillator prepared in the coherent state $|\alpha\rangle$ with the amplitude $\alpha = (3 + 3i)/\sqrt{2}$ performed by the “cat gate” at $n = 4$ and (a) $y_m = x_0 = 3$; (b) $y_m = 2$; (c) $y_m = 1$. The uncertainty region of the input coherent state $(x - 3)^2 + (p - 3)^2 \leq 1$ is magenta colored, whereas its images are orange colored. It is demonstrated that distortions of the input state copies enhance with deviation of the measurement result y_m from the value x_0 representing the coordinate of the point where the initial support region for target oscillator is localized.

can be interpreted as the classical probability of obtaining the measurement outcome y_m at the value of the ancilla coordinate in the vicinity of the overlap points $x_a^{(\pm)} \equiv \pm\sqrt{2n+1 - (y_m - x)^2}$ of the horizontal line $p_a^{(\text{out})} = y_m$ with the resource curve $(p_a^{(\text{out})} - x)^2 + x_a^2 = 2n+1$ (see Fig. 2(b)).

The exponential factors in Eq. (6) provide the symmetrical displacement of the output state components in phase space along the momentum axis by $\delta p(x)$. Substituting Eq. (7) into the momentum produced by the gate in the semiclassical added factor (6) gives the factor in the following explicit form:

$$\varphi_{\text{scl}}(n, z) \sim \frac{1}{(1 - z^2)^{1/4}} [e^{i\phi(n, z)} + (-1)^n e^{-i\phi(n, z)}], \quad (9)$$

where

$$\phi(n, z) \equiv \frac{1}{2}(2n+1) \left(z\sqrt{1-z^2} + \arcsin z \right), \quad (10)$$

$$z \equiv \frac{x - y_m}{\sqrt{2n+1}}. \quad (11)$$

III. EXACT OUTPUT STATE

In the Schrödinger representation, the action of the non-Gaussian gate schematically depicted in Fig. 1 can be described based on the von Neumann reduction postulate. This consideration yields an exact analytic expression for the output wave function of the target oscillator initially prepared in a quantum state that, in the coordinate representation, is given by

$$|\psi_t^{(\text{in})}\rangle = \int dx \psi^{(\text{in})}(x)|x\rangle, \quad (12)$$

where $\psi^{(\text{in})}(x)$ is the wave function of the input state. The ancillary oscillator is prepared in the Fock state with n photons

$$|\psi_a\rangle = \int dx_2 \psi^{(n)}(x_2)|x_2\rangle \quad (13)$$

with the wave function

$$\psi^{(n)}(x_2) = \frac{1}{\pi^{1/4}\sqrt{2^n n!}} H_n(x_2) e^{-x_2^2/2}, \quad (14)$$

where $H_n(x_2)$ is the Hermite polynomial.

Then a two-mode entangling QND operation $C_Z = \exp(iqq_a)$ is applied to the composite system state $|\psi_t\rangle \otimes |\psi_a\rangle$ and a projective ancilla momentum measurement is performed with outcome $p_a^{(\text{out})} = y_m$, resulting in a reduction of the total state to the output state of the target oscillator state (see Ref. [97] for details). The closed-form expression for the wave function of the output state reads

$$\psi^{(\text{out})}(x, y_m) = \frac{1}{\sqrt{N}} \tilde{\psi}^{(\text{out})}(x, y_m), \quad (15)$$

$$\begin{aligned} \tilde{\psi}^{(\text{out})}(x, y_m) &= \psi^{(\text{in})}(x) \\ &\times \frac{(-i)^n}{\pi^{1/4}\sqrt{2^n n!}} H_n(y_m - x) e^{-(y_m - x)^2/2}, \end{aligned} \quad (16)$$

where $\tilde{\psi}^{(\text{out})}(x, y_m)$ is the unnormalized output wave function of the target oscillator and N is the normalization factor. Formulas (15) and (16) define the state that will be referred to as the *exact output state*.

Note that, similar to the semiclassical formula (5), the output wave function is obtained by multiplying the input wave function by the factor representing the gate action. This factor is solely determined by the initial state of the ancilla and the difference between the variables x and y_m while remaining independent of the initial state of the target oscillator. The solution (15) can be expressed in terms of the Fourier transform

F of the Fock state wave function

$$\psi^{(\text{out})}(x, y_m) \sim \psi^{(\text{in})}(x)[F\psi^{(n)}](y_m - x), \quad (17)$$

so that the gate induced factor is the Fourier transform of the resource state coordinate wave function corresponding to the value of momentum $y_m - x$. In the geometric representation shown in Fig. 2, the latter is consistent with the upward shift of x in the circle representing the Fock resource state on the phase plane (see top row of (b) column in Fig. 2).

In the next section we demonstrate that, when the input state is a Glauber coherent state and the value of the measurement outcome is optimal, the exact output state (15) will be close to the Schrödinger cat state with high fidelity regardless of the photon number of the resource Fock state.

IV. GENERATION OF CAT-LIKE STATES FROM COHERENT STATE

In this section, we consider the conditional generation of the Schrödinger cat state via the ‘‘cat gate’’ described above and concentrate on the special case where the initial state of the target oscillator is the Glauber coherent state $|\alpha_0\rangle$ with the amplitude $\alpha_0 = (x_0 + ip_0)/\sqrt{2}$, whereas the ancillary one is still assumed to be prepared in the n -photon Fock state. In the qp phase space, the coherent state $|\alpha_0\rangle$ can be represented by the uncertainty (localization) region bounded by the circle of the radius $\delta x \sim 1/\sqrt{2}$ centered at the point (x_0, p_0) . In this case, the wave function of the input state is

$$\begin{aligned} \psi^{(\text{in})}(x) &= \langle x|\alpha_0\rangle = \psi_{vac}(x - x_0) \exp\{ip_0x - ip_0x_0/2\} \\ &= \pi^{-1/4} \exp\{-(x - x_0)^2/2 + ip_0x - ip_0x_0/2\}, \end{aligned} \quad (18)$$

where ψ_{vac} is the vacuum wave function in the coordinate representation, and Figure 4 schematically shows the semiclassical input-output mapping of the quadrature amplitudes of the target and auxiliary oscillators predicting an emergence of the output state in the form of a cat-like superposition of two ‘‘copies’’ of the input target state.

In Fig. 5, we compare the Wigner function of the exact output state (15)

$$\begin{aligned} W(x, p) &= \frac{1}{\pi} \int dz \psi^{(\text{out})*}(x + z, y_m) \\ &\times \psi^{(\text{out})}(x - z, y_m) e^{2ipz} \end{aligned} \quad (19)$$

computed for the input coherent state (18) with the appropriate semiclassical mapping of the phase space region corresponding to the Gaussian function (18) performed by the gate according to the Eq. (4). Calculations were performed at $y_m = 0$ for the photon number $n = 10$ with $x_0 \in \{0, 1, 2\}$ assuming that the uncertainty region radius of the mapped coherent state is unity. For calculating the Wigner functions, we have developed the fast and efficient method which is based on the technique of generating functions and, thus, avoids performing time consuming numerical integration. Details on this method are relegated to Appendix A.

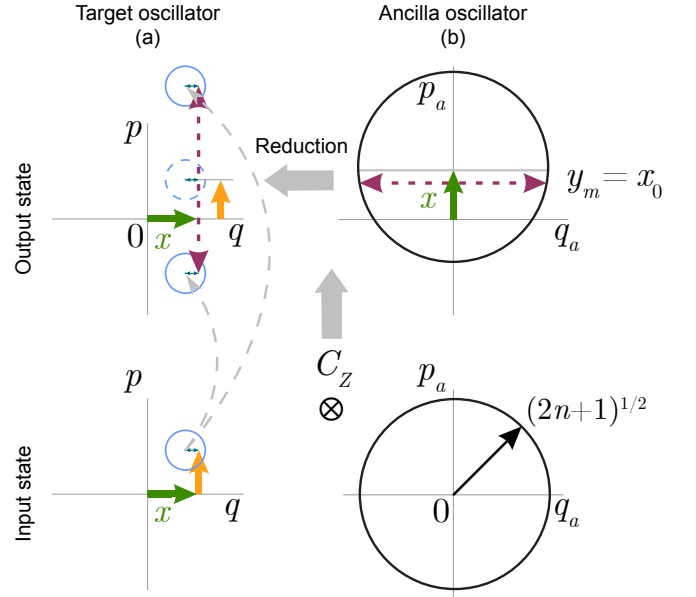


Figure 4. Schematic representation of the measurement-induced two-node ‘‘cat gate’’ operation using the Fock state as an elementary non-Gaussian resource, the entangling C_Z operation, and the projecting homodyne measurement, in the form of semiclassical mapping of the quadrature amplitudes of the target q, p [(a) column] and ancilla q_a, p_a [(b) column] oscillators on the phase plane when the target oscillator is initially prepared in a coherent state $|\alpha_0\rangle$ with amplitude $\alpha_0 = (x_0 + ip_0)/\sqrt{2}$ depicted by an uncertainty disc centered at the point (x_0, p_0) [bottom row of (a) column], and the ancilla in the Fock state with the number of photons n represented by a circle of radius $\sqrt{2n+1}$ in phase space [bottom row of (b) column]. As a result of applying the two-mode entangling operator C_Z and carrying out a homodyne measurement of the ancilla momentum with the outcome y_m , the Fock state-based gate conditionally generates a Schrödinger cat state—a two-component cat-like superposition state, the components of which are symmetrically displaced in phase space along the momentum axis by $x_a^{(\pm)} = \pm\sqrt{2n+1} - (y_m - x)^2$, where x is the initial coordinate of the target oscillator [the top row of (a) column]. The Schrödinger cat state arises when two values of the target oscillator momentum correspond to the measurement result y_m .

Referring to Fig. 5, results for the Wigner functions and the semiclassical mapping are in good agreement. Thus, a simple geometric representation in the phase space based on the semiclassical description can reproduce the output state with high accuracy and also predict the appearance of a minimum disturbed cat-like superposition at the gate output (see the left column in Fig. 5).

Given the input state, from Eqs. (5) and (9), we can construct the semiclassical wave function at the gate output

$$\psi_{\text{scl}}^{(\text{out})}(x, y_m) \sim \psi^{(\text{in})}(x)[e^{i\phi(n,z)} + (-1)^n e^{-i\phi(n,z)}], \quad (20)$$

where $\phi(n, z)$ is the phase function given by Eq. (10), and calculate the fidelity F_{scl} between the semiclassical and exact

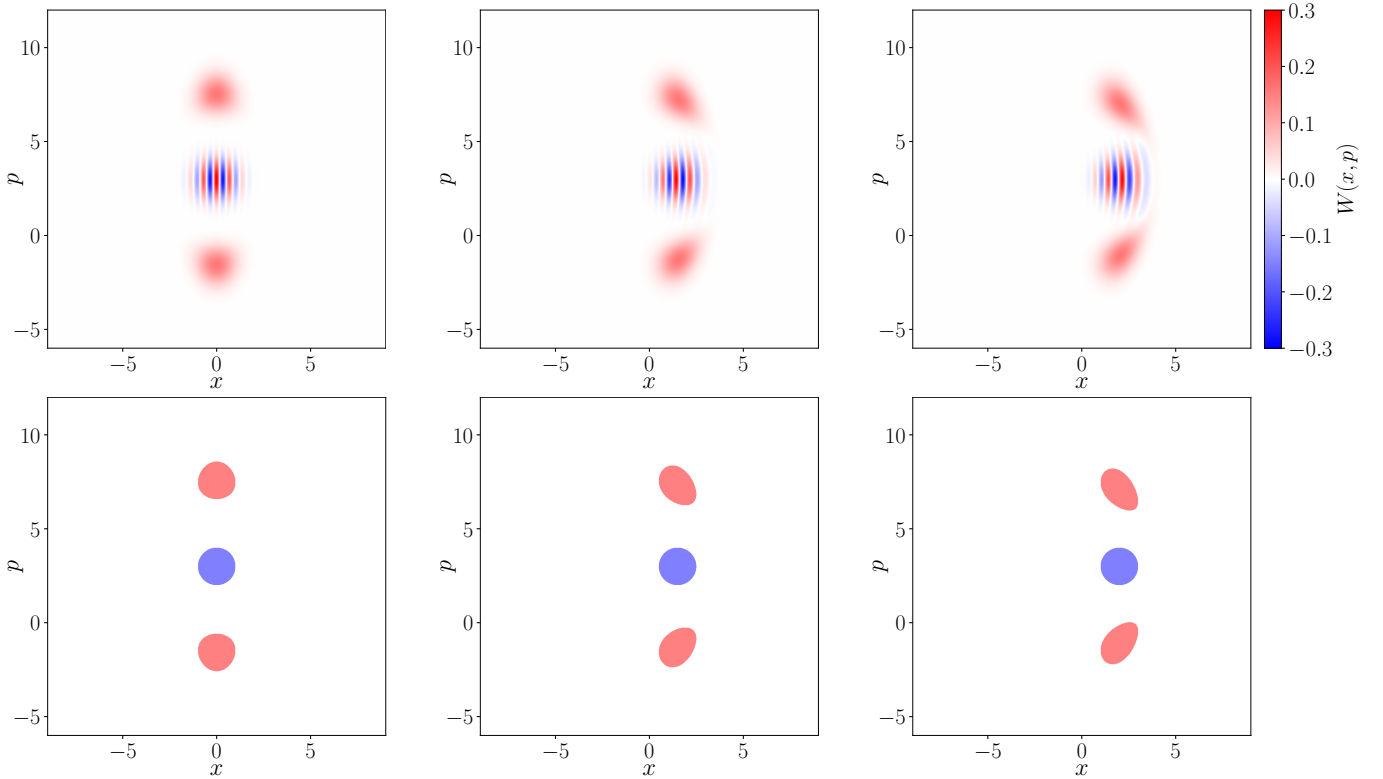


Figure 5. The (top row) Wigner function of the exact output state (15) and (bottom row) semiclassical mapping of the quadrature amplitudes of the target oscillator (see Eq. (4)) at $n = 10$ and $y_m = 0$ for the input coherent state (18) with $p_0 = 3$ and (left column) $x_0 = 0$; (central column) $x_0 = 1.5$; (right column) $x_0 = 2$. The radius of the uncertainty region for the input coherent state is unity. See also the caption of Fig. 3.

output states

$$F_{\text{scl}}(y_m, x_0, n) = \left| \int dx \psi^{(\text{out})*}(x, y_m) \psi_{\text{scl}}^{(\text{out})}(x, y_m) \right|^2. \quad (21)$$

Note that, for the input wave function (18), this fidelity is independent of p_0 .

The plots of F_{scl} computed in relation to the photon number n of the resource state at $y_m = 0$ and different values canonical variable x_0 are shown in Fig. 6. It is seen that the exact output state and the output state recovered from the semiclassical theory are in perfect agreement at small x_0 , namely, with fidelity $F_{\text{scl}} > 0.9970$ at $x_0 = 0$ for any n , $F_{\text{scl}} > 0.9733$ at $x_0 = 1$ for any n , $F_{\text{scl}} > 0.9056$ at $x_0 = 2$ for $n \geq 2$.

In subsequent sections, we shall use formula (20) to deduce the expression for the semiclassical wave function of a Schrödinger cat-like superposition of two “copies” of the initial target state representing the state closest to the exact output state (15) for an arbitrary coherent input state.

A. Schrödinger cat-like state when the input wave function is localized near zero

We begin with the case of cat state generation by the Fock state-based gate when the input state in the phase space occupies

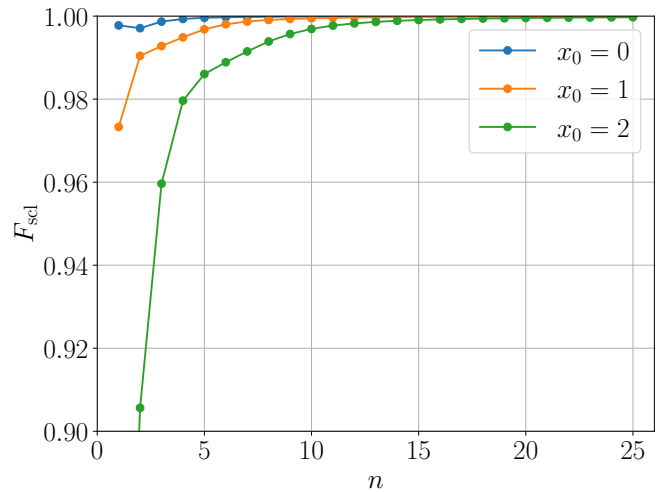


Figure 6. Fidelity F_{scl} between the exact output state (15) and the semiclassical cat (20) as a function of the photon number n of the ancillary oscillator state at $y_m = 0$ for the input coherent state with different values of x_0 .

a limited range of the coordinate near the point $x_0 = 0$, i.e., $x \approx x_0 \ll \sqrt{2n+1}$. Under this assumption, the weighting

factor in Eq. (9) can be assumed constant, and the function $\phi(n, z)$ can be decomposed into a Taylor series in powers of x , which converges at $|x| < \sqrt{2n+1}$ provided that $|y_m| \ll \sqrt{2n+1}$. For $x \ll \sqrt{2n+1}$, we can limit ourselves to the first few terms of the Taylor series for phase ϕ . So, up to the second order in the coordinate x , we have

$$\phi(n, z) \approx \theta + p^{(+)}x + \delta p^{(+)}x^2, \quad (22)$$

where

$$\begin{aligned} \theta &\equiv \phi(n, -y_m/\sqrt{2n+1}), \quad p^{(+)} \equiv \sqrt{2n+1-y_m^2}, \\ \delta p^{(+)} &\equiv \frac{y_m}{2\sqrt{2n+1-y_m^2}}. \end{aligned} \quad (23)$$

When the measurement result $y_m = 0$ the Taylor series (22) can be written up to a linear term in the coordinate x . This approximation yields the gate output state in the form

$$\psi_{\text{cat}}^{(\text{out})}(x) \sim \psi^{(\text{in})}(x)[e^{i(\theta+p^{(+)}x)} + (-1)^n e^{-i(\theta+p^{(+)}x)}], \quad (24)$$

which corresponds to the ‘‘perfect’’ Schrödinger cat state, namely a superposition of two undistorted copies of the target oscillator initial state symmetrically shifted in the phase $q - p$ space along the momentum axis by $\pm p^{(+)} = \pm\sqrt{2n+1}$, with the phase $\theta = 0$. Such semiclassical ‘‘perfect’’ cat state may be represented in terms of a superposition of the Glauber coherent states $|\alpha_+\rangle$ and $|\alpha_-\rangle$,

$$|\psi_{\text{cat}}^{(\text{out})}\rangle = \frac{1}{\sqrt{\mathcal{N}}}[e^{i\theta}|\alpha_+\rangle + (-1)^n e^{-i\theta}|\alpha_-\rangle], \quad (25)$$

where $\alpha_{\pm} = [x_0 + i(p_0 \pm p^{(+)})]/\sqrt{2}$ and \mathcal{N} is the normalization factor.

The terms of the second order and higher concerning x in the Taylor series of the added factor phase $\phi(n, z)$, indicate the dependence of the momentum transmitted by the gate on the target oscillator coordinate x and lead to a distortion of the shape of the region on the phase plane where the Wigner function component is localized. In the geometrical description (see Figs. 2 and 4), this dependence follows from the fact that, for a given measurement outcome y_m , the intersection points $x_a^{(\pm)}$ are displaced when the resource curve is shifted along the vertical axis in changing the coordinate x of the target oscillator if the resource curve is not a vertical line at the intersection with the horizontal line $p_a = y_m$. This results in the copies of the input state of the target oscillator undergo shear deformation of the opposite sign due to the nearly linear dependence of the displacement on x for large enough measurement outcomes y_m , which is described by the quadratic term in the Taylor expand of $\phi(n, z)$ and characterized by the measure of the linear shear deformation being $y_m/(2\sqrt{2n+1-y_m^2})$, as follows from Eq. (23).

In order to evaluate the ‘‘closeness’’ of the exact output state to the Schrödinger cat state, we consider the fidelity

$$F_{\text{cat}}(y_m, x_0, n) = \left| \int dx \psi^{(\text{out})*}(x, y_m) \psi_{\text{cat}}^{(\text{out})}(x) \right|^2. \quad (26)$$

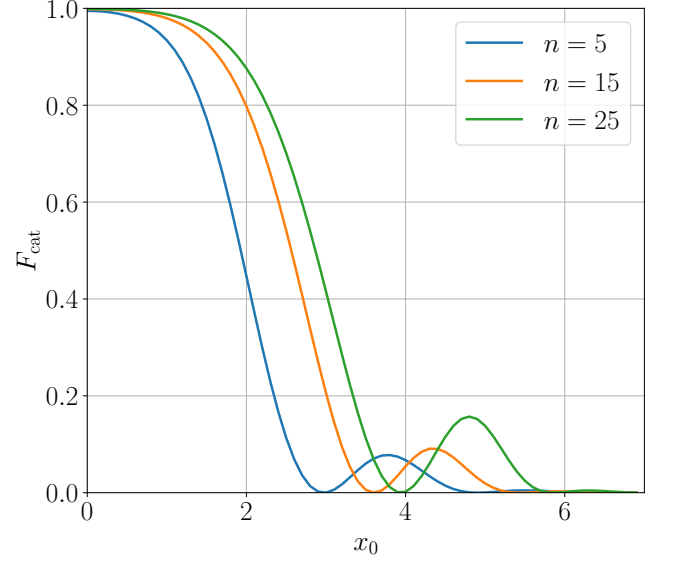


Figure 7. Fidelity F_{cat} (26) between the exact output state (15) and the undisturbed semiclassical cat (24) for the input coherent state (18) as a function of x_0 at the measurement outcome $y_m = 0$ and the photon number $n \in \{5, 15, 25\}$ of the Fock resource state. Fidelity F_{cat} is an even function of x_0 .

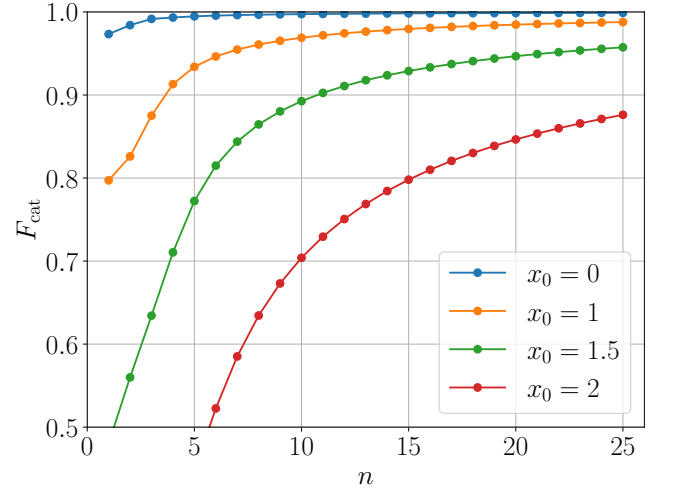


Figure 8. Fidelity F_{cat} (26) between the exact output state (15) and the ‘‘perfect’’ semiclassical cat (24) versus the photon number n of the ancillary oscillator state at the measurement outcome $y_m = 0$ for the input coherent state (18) with $x_0 \in \{0, 1, 1.5, 2\}$.

between the state (15) and the ‘‘perfect’’ cat state (24) recovered from the semiclassical picture.

From the explicit expressions for the wave functions $\psi^{(\text{out})}(x, y_m)$ and $\psi_{\text{cat}}^{(\text{out})}(x)$, it is not difficult to conclude that F_{cat} does not depend on the coordinate y_0 . In Fig. 7, F_{cat} is plotted against x_0 at $y_m = 0$ for various values of the photon

number. It shown that the fidelity reaches unity at $x_0 = 0$ for any value of n . So, F_{cat} remains close to unity only for such coherent states where x_0 lies in the vicinity of the origin. It can also be seen that the fidelity rapidly drops with x_0 .

The Wigner functions of the exact solution (15) at $y_m = 0$ for the input coherent state with $x_0 \in \{0, 1.5, 2\}$ pictured in the top row Fig. 5 demonstrate that, for the resource Fock state with $n = 10$, the output state is close to the undisturbed Schrödinger-cat-like superposition (24) at $x_0 = 0$ in agreement with the curves for F_{cat} (26) plotted in Figs. 7 and 8. Note that, for the columns shown in Fig. 5, the values of the fidelity F_{cat} are: 0.9974 (left column), 0.8926 (central column) and 0.704 (right column).

B. Schrödinger cat-like state when the input wave function is localized away from zero

From Figs. 7 and 8, at the measurement outcome $y_m = 0$, the fidelity F_{cat} between the exact solution (15) and the “perfect” semiclassical cat (24) for the input state (18) is close to unity when the x -quadrature of the input coherent state amplitude x_0 is in the immediate vicinity of zero. It is expected that the size of the vicinity is of the order of vacuum fluctuations level $\delta x = 1/\sqrt{2}$, i.e., $|x_0| \leq \delta x$ (the maximum magnitude for x_0 can be chosen based on the requirements for the value of F_{cat}).

However, the fidelity F_{cat} rapidly declines with x_0 and one of the reasons for this significant reduction is that the wave function (24) of the semiclassical cat state obtained in the previous subsection fails to give a good approximation for the output state (15) provided that the magnitude of x_0 exceeds δx .

In this section, we give a prescription for constructing the Schrödinger cat state closest to the exact output state for the general case when the coherent state (18) with $x_0 \neq 0$ is sent to the input of the Fock state-based gate. In other words, the support of the input wave function $\psi^{(\text{in})}(x)$ is now localized in the vicinity of the point x_0 which is well separated from the origin of the phase space

To construct a cate-like superposition state giving a high fidelity approximation of the exact output state, we expand the phase (10) in the added factor φ_{scl} in a Taylor series in the localization region of the Gaussian $\psi^{(\text{in})}(x)$ as was performed in the previous subsection, i.e., now in the vicinity of the point $x = x_0$. By analogy with (22), in the region $|x - x_0| < \sqrt{2n+1}$ under the condition $|x - y_m| \ll \sqrt{2n+1}$ we expand the phase function $\phi(n, z)$ into the Taylor series in powers of $x - x_0$. In the sufficiently small neighborhood of x_0 with $|x - x_0| \ll \sqrt{2n+1}$, the expansion of the function $\phi(n, z)$ can be truncated up to the second order terms quadratic in $x - x_0$. So, we have

$$\varphi_{\text{scl}} \sim e^{i\phi(n,z)} + (-1)^n e^{-i\phi(n,z)}, \quad (27)$$

$$\phi(n, z) \approx \theta_0 + p_0^{(+)} \cdot (x - x_0) + \delta p_0^{(+)} \cdot (x - x_0)^2, \quad (28)$$

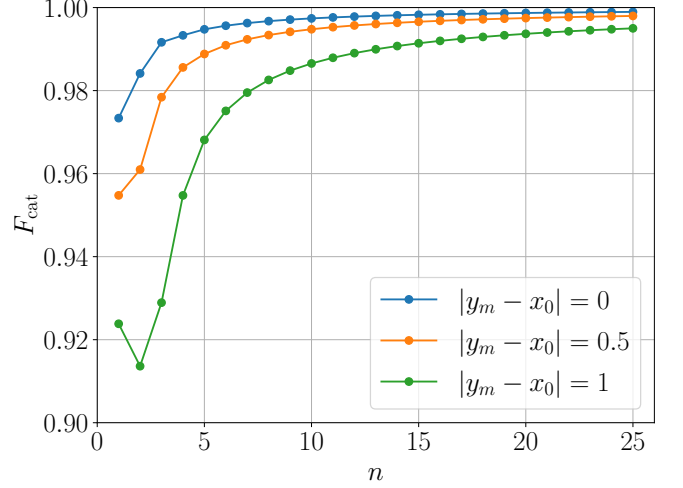


Figure 9. Plot of the fidelity F_{cat} between the exact output state (15) and the “perfect” semiclassical cat state (32) at $x_0 = 1$, shown as a function of the photon number n of the ancillary oscillator state for different values of $y_m = \{0, 1, 1.5\}$.

where

$$\theta_0 = \phi(n, (x_0 - y_m)/\sqrt{2n+1}), \quad (29)$$

$$p_0^{(+)} = \sqrt{2n+1 - (x_0 - y_m)^2}, \quad (30)$$

$$\delta p_0^{(+)} = -\frac{x_0 - y_m}{2\sqrt{2n+1 - (x_0 - y_m)^2}}. \quad (31)$$

At $\delta p_0^{(+)} = 0$ when the measurement result of the ancillary oscillator is $y_m = x_0$, the approximate gate output state (5) with the semiclassical factor determined by formulas (27)–(31) will be the undistorted semiclassical Schrödinger cat given by

$$\psi_{\text{cat}}^{(\text{out})}(x, x_0) \sim \psi^{(\text{in})}(x) [e^{i(\phi_0 + p_0^{(+)} x)} + (-1)^n e^{-i(\phi_0 + p_0^{(+)} x)}], \quad (32)$$

where

$$\phi_0 \equiv -p_0^{(+)} x_0, \quad p_0^{(+)} = \sqrt{2n+1}. \quad (33)$$

In terms This “perfect” Schrödinger cat can also be written as a superposition of Glauber coherent states of the form:

$$|\psi_{\text{cat}}^{(\text{out})}\rangle \sim e^{i\phi_0} |\tilde{\alpha}_+\rangle + (-1)^n e^{-i\phi_0} |\tilde{\alpha}_-\rangle, \quad (34)$$

where $\tilde{\alpha}_{\pm} \equiv [x_0 + i(p_0 \pm p_0^{(+)})]/\sqrt{2}$.

From relations (15), (16), and (32), the fidelity between $\psi_{\text{cat}}^{(\text{out})}(x, y_m)$ and $\psi_{\text{cat}}^{(\text{out})}(x, x_0)$ at $y_m = x_0$

$$F_{\text{cat}}(n) = \left| \int dx \psi_{\text{cat}}^{(\text{out})\ast}(x, x_0) \psi_{\text{cat}}^{(\text{out})}(x, x_0) \right|_{y_m=x_0}^2 \quad (35)$$

is independent of both p_0 and x_0 (since the integrand depends only on the difference $x - x_0$ and the integral is taken over

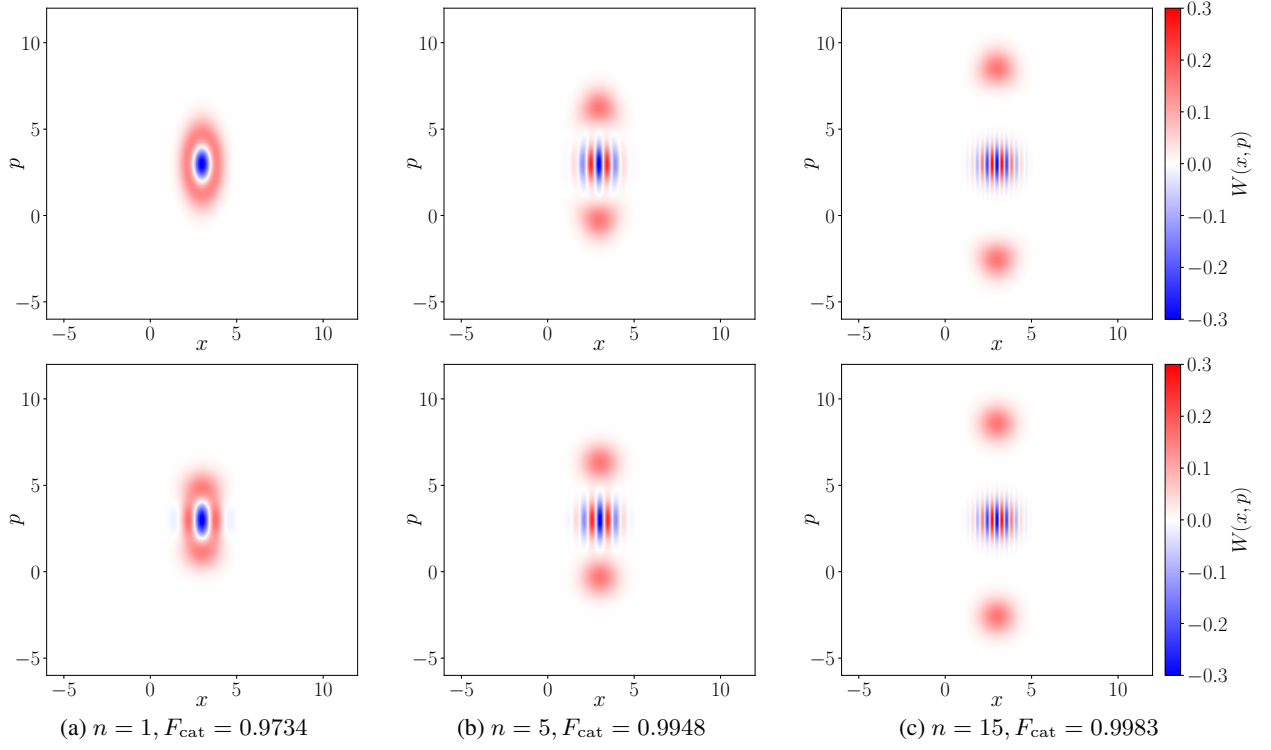


Figure 10. Wigner functions of the (top row) exact output state (15) and (bottom row) “perfect” semiclassical cat (32) obtained from the input coherent state with amplitude $\alpha_0 = (3 + 3i)/\sqrt{2}$ corresponding to the measurement result $y_m = x_0 = 3$ for the Fock resource state with the photon number (a) $n = 1$; (b) $n = 5$, (c) $n = 15$. F_{cat} is the fidelity between the corresponding states.

an unbounded interval) and, thus, is determined solely by the photon number n .

Note that from the semiclassical description it can be inferred the output state created by the scheme under consideration from the coherent state $|\alpha_0\rangle$ with the amplitude $\alpha_0 = (x_0 + ip_0)/\sqrt{2}$, at $y_m = x_0$, will be close to the “perfect” cat (32) with high fidelity for any photon number of the resource state because target state is localized in proximity of x_0 with the characteristic length $\delta x \sim 1/\sqrt{2}$. Therefore, for all x belonging to the input function support, the semiclassical relation $|x - x_0| \ll \sqrt{2n + 1}$ will be fulfilled, which guarantees the generation of an undistorted cat state.

Fig. 9 illustrates that an increase in the difference $|y_m - x_0|$ has a detrimental effect on the fidelity. The curves for the fidelity (35) plotted in Fig. 9 show that the quality of the semiclassical approximation given by Eq. (34) improves as the photon number n increases. This conclusion is also illustrated in Fig. 10 where, for $y_m = x_0 = 3$ and $n \in \{1, 5, 15\}$, the Wigner functions of the exact output state (15) are compared with their semiclassical counterparts computed for the undeformed cat (32).

Statistics of the homodyne measurements of the ancilla momentum is described by the probability density to observe the outcome y_m given by the norm of the unnormalized output wave function (16)

$$P(y_m) = \langle \tilde{\psi}^{(\text{out})} | \tilde{\psi}^{(\text{out})} \rangle = \int dx |\tilde{\psi}^{(\text{out})}(x, y_m)|^2, \quad (36)$$

so that the wave function (15) of the output state can be written

as

$$\psi^{(\text{out})}(x, y_m) = \frac{\tilde{\psi}^{(\text{out})}(x, y_m)}{\sqrt{P(y_m)}}. \quad (37)$$

For the input coherent state (18) of the target oscillator and the Fock resource state (13) with n photons, the probability density takes the explicit form

$$\begin{aligned} P(y_m, x_0) &= \frac{1}{\pi 2^n n!} \int dx |H_n(y_m - x)|^2 e^{-(y_m - x)^2} e^{-(x - x_0)^2} \\ &= P(y_m - x_0, 0) = P(x_0 - y_m, 0) \end{aligned} \quad (38)$$

where the probability density $P(y_m, 0)$ corresponds to the vacuum state of the target oscillator [97]. Note that $P(y_m, 0)$ is even in y_m due to the parity in ξ of the absolute value of the Hermite polynomials $|H_n(\xi)|$. In Fig. 11, the probability density $P(y_m, 0)$ is plotted as a function of y_m at different values of the photon number. It is seen that each curve for $P(y_m, 0)$ has the local maximum value that decreases with n .

Since, in real-world experiments, the measurement outcome can only be identified with a certain precision, it is instructive to consider a mixed output state that emerges when the observed ancilla momentum falls within an acceptance interval ranged from $-d/2$ to $d/2$ of the width d centered at $y_m = 0$ provided $x_0 = 0$. In this case, the weighted fidelity between the “perfect” semiclassical cat state (24) and the mixed state at the gate output

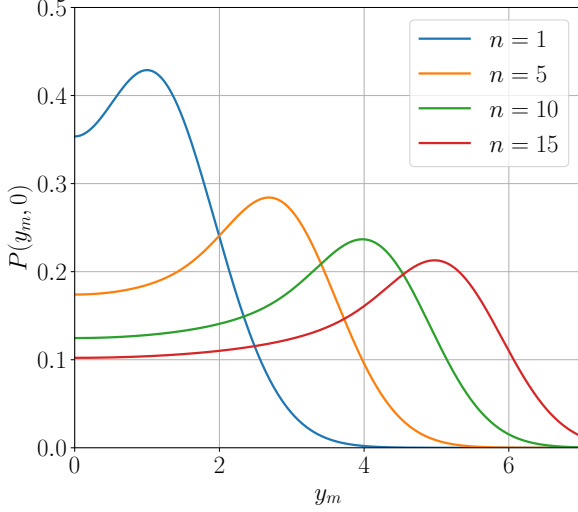


Figure 11. The probability density $P(y_m, 0)$ in relation to the ancilla momentum measurement outcome y_m at different values of the photon number $n \in \{1, 5, 10, 15\}$ of the Fock resource state for the input coherent state with $x_0 = 0$. $P(y_m, 0)$ is an even function of y_m and $P(y_m, x_0) = P(y_m - x_0, 0)$.

is evaluated as follows

$$F^{\text{mix}}(d) = \frac{1}{P^{\text{mix}}(d)} \int_{-d/2}^{+d/2} dy_m P(y_m, 0) F_{\text{cat}}(y_m), \quad (39)$$

where $P^{\text{mix}}(d) \equiv \int_{-d/2}^{+d/2} dy_m P(y_m, 0)$ is the probability that the measurement outcome is within the acceptance interval.

When $x_0 \neq 0$, we choose the acceptance interval to be centered at $y_m = x_0$ and insert the ideal cat (32) into the expression for $F_{\text{cat}}(y_m)$. After change of the variable: $x \rightarrow x - x_0$, the expression for $F^{\text{mix}}(d)$ is reduced to Eq. (39).

Figure 12 presents the results for the fidelity $F^{\text{mix}}(d)$ evaluated as a function of the acceptance interval length, d , at different values of the photon number, $n \in \{1, 5, 10\}$. From Fig. 12 it is essential to use sufficiently narrow acceptance intervals in order to prepare a mixed state with high fidelity $F^{\text{mix}}(d)$ to the undistorted semiclassical cat state (24).

It is useful to note that, for small intervals with $d \ll \sqrt{2n+1}$, the probability that the measurement outcome lies in the acceptance interval is proportional to d and can be estimated as $P^{\text{mix}}(d) \approx P(0, 0)d$. This behavior comes from the weak dependence of the probability density on y_m at low y_m (see Fig. 11).

V. DISCUSSIONS AND CONCLUSION

We have studied the CV measurement-induced Fock state-based ‘‘cat gate’’ which can conditionally generate a two-component Schrödinger cat-like superposition from the input coherent state. It is shown that the geometric semiclassical

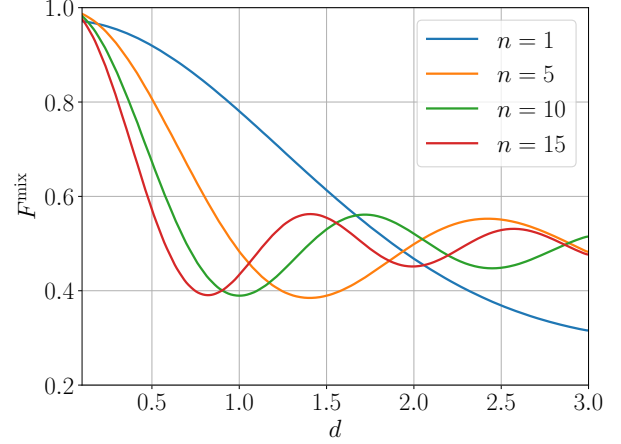


Figure 12. Fidelity F^{mix} (see Eq. (39)) between the output mixed state and the ‘‘perfect’’ semiclassical cat state (24) of the target oscillator as a function of the acceptance interval d at $n \in \{1, 5, 10, 15\}$.

mapping in the phase space can be used to evaluate such important characteristics as the number of components of the cat-like superposition, their positions, and distortions produced by the logical element. We have identified the gate operation regime, where the output state is close to the ‘‘perfect’’ semiclassical Schrödinger cat state represented by the superposition of two undeformed copies of the input state symmetrically displaced in the phase space. The ‘‘size’’ of the generated Schrödinger cat at the gate output - the ‘‘distance’’ between the copies - can be made as large as required by an appropriate choice of the gate parameters. A key feature of the gate under consideration is that the Schrödinger cat state emerges when the ancillary oscillator measurement is compatible with multiple values of the target oscillator physical variables.

We have performed a detailed analysis of the fidelity between the gate output state and ‘‘perfect’’ Schrödinger cat state derived from semiclassical theory. We have found the criteria for the gate operation with high fidelity values exceeding 0.99 (see Fig. 9) for a coherent state at the gate input and have illustrated the qualitative features of the output cat states in terms of their Wigner functions depending on the gate parameters and measurement outcome. A clear interpretation of the output state quantum statistics in terms of the Wigner function in dependence on the gate parameters and measurement outcome was presented.

In analogy to some other non-Gaussian CV schemes, the studied ‘‘cat gate’’ uses the same key elements such as the Fock resource state, the entangling C_Z operation, and the homodyne measurement. A key feature of the regime where the cat-like superposition emerges is that the projective measurement provides multivalued information about the target system’s physical variables. From our analysis, it might be concluded that this feature may arise in CV quantum networks with embedded non-Gaussian gates of a general kind using more complex resource states and other types of measurements that may cause measurement-induced evolution leading to the generation of

the multi-component Schrödinger cat states which can be used as the logical qubit basis for error correction codes. The cat-breeding transformations of an arbitrary input state may be combined with standard Gaussian operations such as displacement, rotation, squeezing, and shear deformation, and can be successfully applied in complex non-Gaussian quantum networks.

ACKNOWLEDGMENTS

N.G.V. is grateful to Dr. Ivan V. Sokolov for the meaningful discussions. The work was supported by Russian Science Foundation (project No. 24-21-00484).

DECLARATION OF COMPETING INTERESTS

The authors declare that they have no known competing financial interests or personal relationships that could have appeared to influence the work reported in this paper.

Data Availability Statement: This manuscript has no associated data or the data will not be deposited. [Authors comment: This is a theoretical study and no experimental data has been listed.]

-
- [1] D. W. Moore, Quantum hypergraph states in continuous variables, *Physical Review A* **100**, [10.1103/physreva.100.062301](https://doi.org/10.1103/physreva.100.062301) (2019).
- [2] S. Konno, A. Sakaguchi, W. Asavanant, H. Ogawa, M. Kobayashi, P. Marek, R. Filip, J.-i. Yoshikawa, and A. Furusawa, Nonlinear squeezing for measurement-based non-gaussian operations in time domain, *Physical Review Applied* **15**, [10.1103/physrevapplied.15.024024](https://doi.org/10.1103/physrevapplied.15.024024) (2021).
- [3] F. Hanamura, W. Asavanant, H. Nagayoshi, A. Sakaguchi, R. Ide, K. Fukui, P. van Loock, and A. Furusawa, Implementing arbitrary multimode continuous-variable quantum gates with fixed non-gaussian states and adaptive linear optics, *Physical Review A* **110**, [10.1103/physreva.110.022614](https://doi.org/10.1103/physreva.110.022614) (2024).
- [4] W. Asavanant, B. Charoensombutamon, S. Yokoyama, T. Ebihara, T. Nakamura, R. N. Alexander, M. Endo, J.-i. Yoshikawa, N. C. Menicucci, H. Yonezawa, and A. Furusawa, Time-domain-multiplexed measurement-based quantum operations with 25-mhz clock frequency, *Physical Review Applied* **16**, [10.1103/physrevapplied.16.034005](https://doi.org/10.1103/physrevapplied.16.034005) (2021).
- [5] M. V. Larsen, X. Guo, C. R. Breum, J. S. Neergaard-Nielsen, and U. L. Andersen, Deterministic multi-mode gates on a scalable photonic quantum computing platform, *Nature Physics* **17**, 1018–1023 (2021).
- [6] S. D. Bartlett and B. C. Sanders, Universal continuous-variable quantum computation: Requirement of optical nonlinearity for photon counting, *Phys. Rev. A* **65**, 042304 (2002).
- [7] J. Niset, J. Fiurášek, and N. J. Cerf, No-go theorem for gaussian quantum error correction, *Physical Review Letters* **102**, [10.1103/physrevlett.102.120501](https://doi.org/10.1103/physrevlett.102.120501) (2009).
- [8] E. Chitambar and G. Gour, Quantum resource theories, *Reviews of Modern Physics* **91**, [10.1103/revmodphys.91.025001](https://doi.org/10.1103/revmodphys.91.025001) (2019).
- [9] J. Lee, J. Park, and H. Nha, Quantum non-gaussianity and secure quantum communication, *npj Quantum Information* **5**, [10.1038/s41534-019-0164-9](https://doi.org/10.1038/s41534-019-0164-9) (2019).
- [10] B. Q. Baragiola, G. Pantaleoni, R. N. Alexander, A. Karanjai, and N. C. Menicucci, All-gaussian universality and fault tolerance with the Gottesman-Kitaev-Preskill code, *Phys. Rev. Lett.* **123**, 200502 (2019).
- [11] U. Chabaud and M. Walschaers, Resources for bosonic quantum computational advantage, *Physical Review Letters* **130**, [10.1103/physrevlett.130.090602](https://doi.org/10.1103/physrevlett.130.090602) (2023).
- [12] A. Ourjoumtsev, R. Tualle-Brouri, and P. Grangier, Quantum homodyne tomography of a two-photon fock state, *Phys. Rev. Lett.* **96**, 213601 (2006).
- [13] H. Lee, P. Kok, N. J. Cerf, and J. P. Dowling, Linear optics and projective measurements alone suffice to create large-photon-number path entanglement, *Physical Review A* **65**, [10.1103/physreva.65.030101](https://doi.org/10.1103/physreva.65.030101) (2002).
- [14] M. Cooper, L. J. Wright, C. Söller, and B. J. Smith, Experimental generation of multi-photon fock states, *Optics Express* **21**, 5309 (2013).
- [15] M. Bouillard, G. Boucher, J. F. Ortas, B. Kanseri, and R. Tualle-Brouri, High production rate of single-photon and two-photon fock states for quantum state engineering, *Optics Express* **27**, 3113 (2019).
- [16] J. Tiedau, T. J. Bartley, G. Harder, A. E. Lita, S. W. Nam, T. Gerrits, and C. Silberhorn, Scalability of parametric down-conversion for generating higher-order fock states, *Phys. Rev. A* **100**, 041802 (2019).
- [17] N. Quesada, L. G. Helt, J. Izaac, J. M. Arrazola, R. Shahrokhshahi, C. R. Myers, and K. K. Sabapathy, Simulating realistic non-gaussian state preparation, *Phys. Rev. A* **100**, 022341 (2019).
- [18] K. Takase, J.-i. Yoshikawa, W. Asavanant, M. Endo, and A. Furusawa, Generation of optical Schrödinger cat states by generalized photon subtraction, *Phys. Rev. A* **103**, 013710 (2021).
- [19] A. Banerji and G. Puentes, *Deterministic preparation of non-gaussian quantum states: Applications in quantum information protocols* (2021).
- [20] M. Walschaers, Non-gaussian quantum states and where to find them, *PRX Quantum* **2**, [10.1103/prxquantum.2.030204](https://doi.org/10.1103/prxquantum.2.030204) (2021).
- [21] V. Kala, R. Filip, and P. Marek, Cubic nonlinear squeezing and its decoherence, *Optics Express* **30**, 31456 (2022).
- [22] M. G. Genoni and M. G. A. Paris, Quantifying non-gaussianity for quantum information, *Physical Review A* **82**, [10.1103/physreva.82.052341](https://doi.org/10.1103/physreva.82.052341) (2010).
- [23] S. Wang, L.-L. Hou, X.-F. Chen, and X.-F. Xu, Continuous-variable quantum teleportation with non-gaussian entangled states generated via multiple-photon subtraction and addition, *Phys. Rev. A* **91**, 063832 (2015).
- [24] F. Arzani, N. Treps, and G. Ferrini, Polynomial approximation of non-gaussian unitaries by counting one photon at a time, *Phys. Rev. A* **95**, 052352 (2017).
- [25] Q. Zhuang, Z. Zhang, and J. H. Shapiro, Optimum mixed-state

- discrimination for noisy entanglement-enhanced sensing, *Phys. Rev. Lett.* **118**, 040801 (2017).
- [26] K. K. Sabapathy and A. Winter, Non-gaussian operations on bosonic modes of light: Photon-added gaussian channels, *Phys. Rev. A* **95**, 062309 (2017).
- [27] Q. Zhuang, P. W. Shor, and J. H. Shapiro, Resource theory of non-gaussian operations, *Physical Review A* **97**, 10.1103/physreva.97.052317 (2018).
- [28] M. Fuwa, S. Toba, S. Takeda, P. Marek, L. Mišta, R. Filip, P. van Loock, J.-i. Yoshikawa, and A. Furusawa, Noiseless conditional teleportation of a single photon, *Physical Review Letters* **113**, 10.1103/physrevlett.113.223602 (2014).
- [29] J. Zhao, H. Jeng, L. O. Conlon, S. Tserkis, B. Shajilal, K. Liu, T. C. Ralph, S. M. Assad, and P. K. Lam, Enhancing quantum teleportation efficacy with noiseless linear amplification, *Nature Communications* **14**, 10.1038/s41467-023-40438-z (2023).
- [30] V. Kala, M. Walschaers, R. Filip, and P. Marek, *Non-gaussian state teleportation with a nonlinear feedforward* (2024).
- [31] H. Takahashi, J. S. Neergaard-Nielsen, M. Takeuchi, M. Takeoka, K. Hayasaka, A. Furusawa, and M. Sasaki, Entanglement distillation from gaussian input states, *Nature Photonics* **4**, 178–181 (2010).
- [32] Y. Mardani, A. Shafiei, M. Ghadimi, and M. Abdi, Continuous-variable entanglement distillation by cascaded photon replacement, *Physical Review A* **102**, 10.1103/physreva.102.012407 (2020).
- [33] F. Hanamura, W. Asavanant, K. Fukui, S. Konno, and A. Furusawa, Estimation of gaussian random displacement using non-gaussian states, *Physical Review A* **104**, 10.1103/physreva.104.062601 (2021).
- [34] X. Wang, M. Xu, Y. Zhao, Z. Chen, S. Yu, and H. Guo, *Non-gaussian reconciliation for continuous-variable quantum key distribution* (2023).
- [35] D. Gottesman, A. Kitaev, and J. Preskill, Encoding a qubit in an oscillator, *Physical Review A* **64**, 10.1103/physreva.64.012310 (2001).
- [36] N. C. Menicucci, P. van Loock, M. Gu, C. Weedbrook, T. C. Ralph, and M. A. Nielsen, Universal quantum computation with continuous-variable cluster states, *Physical Review Letters* **97**, 10.1103/physrevlett.97.110501 (2006).
- [37] B.-H. Wu, R. N. Alexander, S. Liu, and Z. Zhang, Quantum computing with multidimensional continuous-variable cluster states in a scalable photonic platform, *Physical Review Research* **2**, 10.1103/physrevresearch.2.023138 (2020).
- [38] T. Yoshida, D. Okuno, T. Kashiwazaki, T. Umeki, S. Miki, F. China, M. Yabuno, H. Terai, and S. Takeda, *Scalable and programmable quantum computing platform for optical non-gaussian input states* (2024).
- [39] R. García-Patrón, J. Fiurášek, N. J. Cerf, J. Wenger, R. Tualle-Brouri, and P. Grangier, Proposal for a loophole-free bell test using homodyne detection, *Physical Review Letters* **93**, 10.1103/physrevlett.93.130409 (2004).
- [40] B. G. Christensen, K. T. McCusker, J. B. Altepeter, B. Calkins, T. Gerrits, A. E. Lita, A. Miller, L. K. Shalm, Y. Zhang, S. W. Nam, N. Brunner, C. C. W. Lim, N. Gisin, and P. G. Kwiat, Detection-loophole-free test of quantum nonlocality, and applications, *Physical Review Letters* **111**, 10.1103/physrevlett.111.130406 (2013).
- [41] I. Georgescu, S. Ashhab, and F. Nori, Quantum simulation, *Reviews of Modern Physics* **86**, 153–185 (2014).
- [42] R. Yanagimoto, E. Ng, L. G. Wright, T. Onodera, and H. Mabuchi, Efficient simulation of broadband non-gaussian quantum optics using matrix product states, in *Conference on Lasers and Electro-Optics*, CLEO_AT, Vol. 91 (Optica Publishing Group, 2022) p. JTu3A.18.
- [43] T. C. Ralph, A. Gilchrist, G. J. Milburn, W. J. Munro, and S. Glancy, Quantum computation with optical coherent states, *Physical Review A* **68**, 10.1103/physreva.68.042319 (2003).
- [44] A. Gilchrist, K. Nemoto, W. J. Munro, T. C. Ralph, S. Glancy, S. L. Braunstein, and G. J. Milburn, Schrödinger cats and their power for quantum information processing, *Journal of Optics B: Quantum and Semiclassical Optics* **6**, S828 (2004).
- [45] A. P. Lund, T. C. Ralph, and H. L. Haselgrove, Fault-tolerant linear optical quantum computing with small-amplitude coherent states, *Phys. Rev. Lett.* **100**, 030503 (2008).
- [46] M. Mirrahimi, Z. Leghtas, V. V. Albert, S. Touzard, R. J. Schoelkopf, L. Jiang, and M. H. Devoret, Dynamically protected cat-qubits: a new paradigm for universal quantum computation, *New Journal of Physics* **16**, 045014 (2014).
- [47] J. S. Neergaard-Nielsen, M. Takeuchi, K. Wakui, H. Takahashi, K. Hayasaka, M. Takeoka, and M. Sasaki, Optical continuous-variable qubit, *Phys. Rev. Lett.* **105**, 053602 (2010).
- [48] N. Sangouard, C. Simon, N. Gisin, J. Laurat, R. Tualle-Brouri, and P. Grangier, Quantum repeaters with entangled coherent states, *Journal of the Optical Society of America B* **27**, A137 (2010).
- [49] J. B. Brask, I. Rigas, E. S. Polzik, U. L. Andersen, and A. S. Sørensen, Hybrid long-distance entanglement distribution protocol, *Physical Review Letters* **105**, 10.1103/physrevlett.105.160501 (2010).
- [50] P. van Loock, N. Lütkenhaus, W. J. Munro, and K. Nemoto, Quantum repeaters using coherent-state communication, *Phys. Rev. A* **78**, 062319 (2008).
- [51] R. Goncharov, A. D. Kiselev, E. Moiseev, E. Samsonov, S. Moiseev, F. Kiselev, and V. Egorov, *Quantum repeaters and teleportation via entangled phase-modulated multimode coherent states* (2023).
- [52] J. Joo, W. J. Munro, and T. P. Spiller, Quantum metrology with entangled coherent states, *Phys. Rev. Lett.* **107**, 083601 (2011).
- [53] W. J. Munro, K. Nemoto, G. J. Milburn, and S. L. Braunstein, Weak-force detection with superposed coherent states, *Physical Review A* **66**, 10.1103/physreva.66.023819 (2002).
- [54] B. Vlastakis, G. Kirchmair, Z. Leghtas, S. E. Nigg, L. Frunzio, S. M. Girvin, M. Mirrahimi, M. H. Devoret, and R. J. Schoelkopf, Deterministically encoding quantum information using 100-photon schrödinger cat states, *Science* **342**, 607 (2013).
- [55] K. C. Tan and H. Jeong, Nonclassical light and metrological power: An introductory review, *AVS Quantum Science* **1**, 10.1116/1.5126696 (2019).
- [56] H. Jeong, M. S. Kim, and J. Lee, Quantum-information processing for a coherent superposition state via a mixed-entangled coherent channel, *Physical Review A* **64**, 10.1103/physreva.64.052308 (2001).
- [57] A. Ourjoumtsev, R. Tualle-Brouri, J. Laurat, and P. Grangier, Generating optical schrödinger kittens for quantum information processing, *Science* **312**, 83 (2006).
- [58] A. Facon, E.-K. Dietsche, D. Grosso, S. Haroche, J.-M. Raimond, M. Brune, and S. Gleyzes, A sensitive electrometer based on a rydberg atom in a schrödinger-cat state, *Nature* **535**, 262 (2016).
- [59] P. A. Knott, T. J. Proctor, A. J. Hayes, J. P. Cooling, and J. A. Dunningham, Practical quantum metrology with large precision gains in the low-photon-number regime, *Physical Review A* **93**, 10.1103/physreva.93.033859 (2016).
- [60] K. Duivenvoorden, B. M. Terhal, and D. Weigand, Single-mode displacement sensor, *Physical Review A* **95**, 10.1103/physreva.95.012305 (2017).

- [61] S. J. van Enk and O. Hirota, Entangled coherent states: Teleportation and decoherence, *Phys. Rev. A* **64**, 022313 (2001).
- [62] S.-W. Lee and H. Jeong, Near-deterministic quantum teleportation and resource-efficient quantum computation using linear optics and hybrid qubits, *Physical Review A* **87**, 10.1103/physreva.87.022326 (2013).
- [63] F. Gaitan, *Quantum Error Correction and Fault Tolerant Quantum Computing* (CRC Press, 2018).
- [64] V. V. Albert, K. Noh, K. Duivendoorn, D. J. Young, R. T. Brierley, P. Reinhold, C. Vuillot, L. Li, C. Shen, S. M. Girvin, B. M. Terhal, and L. Jiang, Performance and structure of single-mode bosonic codes, *Physical Review A* **97**, 10.1103/physreva.97.032346 (2018).
- [65] A. L. Grimsmo, J. Combes, and B. Q. Baragiola, Quantum computing with rotation-symmetric bosonic codes, *Physical Review X* **10**, 10.1103/physrevx.10.011058 (2020).
- [66] W. Cai, Y. Ma, W. Wang, C.-L. Zou, and L. Sun, Bosonic quantum error correction codes in superconducting quantum circuits, *Fundamental Research* **1**, 50–67 (2021).
- [67] C. Chamberland, K. Noh, P. Arrangoiz-Arriola, E. T. Campbell, C. T. Hann, J. Iverson, H. Putterman, T. C. Bohdanowicz, S. T. Flammia, A. Keller, G. Refael, J. Preskill, L. Jiang, A. H. Safavi-Naeini, O. Painter, and F. G. Brandão, Building a fault-tolerant quantum computer using concatenated cat codes, *PRX Quantum* **3**, 10.1103/prxquantum.3.010329 (2022).
- [68] J. Etesse, R. Blandino, B. Kanseri, and R. Tualle-Brouri, Proposal for a loophole-free violation of bell's inequalities with a set of single photons and homodyne measurements, *New Journal of Physics* **16**, 053001 (2014).
- [69] J. Etesse, M. Bouillard, B. Kanseri, and R. Tualle-Brouri, Experimental generation of squeezed cat states with an operation allowing iterative growth, *Phys. Rev. Lett.* **114**, 193602 (2015).
- [70] D. V. Sychev, A. E. Ulanov, A. A. Pushkina, M. W. Richards, I. A. Fedorov, and A. I. Lvovsky, Enlargement of optical schrödinger's cat states, *Nature Photonics* **11**, 379 (2017).
- [71] W. H. Zurek, Sub-planck structure in phase space and its relevance for quantum decoherence, *Nature* **412**, 712–717 (2001).
- [72] C. C. Gerry and P. L. Knight, Quantum superpositions and schrödinger cat states in quantum optics, *American Journal of Physics* **65**, 964–974 (1997).
- [73] W. P. Schleich, *Quantum Optics in Phase Space* (Wiley, 2001).
- [74] W. Qin, A. Miranowicz, H. Jing, and F. Nori, Generating long-lived macroscopically distinct superposition states in atomic ensembles, *Physical Review Letters* **127**, 10.1103/physrevlett.127.093602 (2021).
- [75] P. T. Cochrane, G. J. Milburn, and W. J. Munro, Macroscopically distinct quantum-superposition states as a bosonic code for amplitude damping, *Phys. Rev. A* **59**, 2631 (1999).
- [76] H. M. Vasconcelos, L. Sanz, and S. Glancy, All-optical generation of states for “encoding a qubit in an oscillator”, *Optics Letters* **35**, 3261 (2010).
- [77] D. J. Weigand and B. M. Terhal, Generating grid states from schrödinger-cat states without postselection, *Physical Review A* **97**, 10.1103/physreva.97.022341 (2018).
- [78] J. Hastrup, J. S. Neergaard-Nielsen, and U. L. Andersen, Deterministic generation of a four-component optical cat state, *Optics Letters* **45**, 640 (2020).
- [79] A. Perez-Leija, A. Szameit, I. Ramos-Prieto, H. Moya-Cessa, and D. N. Christodoulides, Generalized schrödinger cat states and their classical emulation, *Physical Review A* **93**, 10.1103/physreva.93.053815 (2016).
- [80] K. Huang, H. Le Jeannic, J. Ruauvel, V. B. Verma, M. D. Shaw, F. Marsili, S. W. Nam, E. Wu, H. Zeng, Y.-C. Jeong, R. Filip, O. Morin, and J. Laurat, Optical synthesis of large-amplitude squeezed coherent-state superpositions with minimal resources, *Phys. Rev. Lett.* **115**, 023602 (2015).
- [81] A. Omran, H. Levine, A. Keesling, G. Semeghini, T. T. Wang, S. Ebadi, H. Bernien, A. S. Zibrov, H. Pichler, S. Choi, J. Cui, M. Rossignolo, P. Rembold, S. Montangero, T. Calarco, M. Endres, M. Greiner, V. Vuletić, and M. D. Lukin, Generation and manipulation of schrödinger cat states in rydberg atom arrays, *Science* **365**, 570–574 (2019).
- [82] C. Song, K. Xu, H. Li, Y.-R. Zhang, X. Zhang, W. Liu, Q. Guo, Z. Wang, W. Ren, J. Hao, H. Feng, H. Fan, D. Zheng, D.-W. Wang, H. Wang, and S.-Y. Zhu, Generation of multicomponent atomic schrödinger cat states of up to 20 qubits, *Science* **365**, 574–577 (2019).
- [83] M. Lewenstein, M. F. Ciappina, E. Pisanty, J. Rivera-Dean, P. Stammer, T. Lamprou, and P. Tzallas, Generation of optical schrödinger cat states in intense laser–matter interactions, *Nature Physics* **17**, 1104 (2021).
- [84] M. Dakna, T. Anhut, T. Opatrný, L. Knöll, and D.-G. Welsch, Generating schrödinger-cat-like states by means of conditional measurements on a beam splitter, *Physical Review A* **55**, 3184 (1997).
- [85] R. Dong, A. Tipsmark, A. Laghaout, L. A. Krivitsky, M. Ježek, and U. L. Andersen, Generation of picosecond pulsed coherent state superpositions, *Journal of the Optical Society of America B* **31**, 1192 (2014).
- [86] T. Gerrits, S. Glancy, T. S. Clement, B. Calkins, A. E. Lita, A. J. Miller, A. L. Migdall, S. W. Nam, R. P. Mirin, and E. Knill, Generation of optical coherent-state superpositions by number-resolved photon subtraction from the squeezed vacuum, *Phys. Rev. A* **82**, 031802 (2010).
- [87] W. Asavanant, K. Nakashima, Y. Shiozawa, J.-I. Yoshikawa, and A. Furusawa, Generation of highly pure schrödinger's cat states and real-time quadrature measurements via optical filtering, *Optics Express* **25**, 32227 (2017).
- [88] H. Takahashi, K. Wakui, S. Suzuki, M. Takeoka, K. Hayasaka, A. Furusawa, and M. Sasaki, Generation of large-amplitude coherent-state superposition via ancilla-assisted photon subtraction, *Phys. Rev. Lett.* **101**, 233605 (2008).
- [89] J. S. Neergaard-Nielsen, B. M. Nielsen, C. Hettich, K. Mølmer, and E. S. Polzik, Generation of a superposition of odd photon number states for quantum information networks, *Phys. Rev. Lett.* **97**, 083604 (2006).
- [90] E. N. Bashmakova, S. B. Korolev, and T. Y. Golubeva, Effect of entanglement in the generalized photon subtraction scheme, *Laser Physics Letters* **20**, 115203 (2023).
- [91] A. Ourjoumtsev, H. Jeong, R. Tualle-Brouri, and P. Grangier, Generation of optical ‘schrödinger cats’ from photon number states, *Nature* **448**, 784 (2007).
- [92] A. Ourjoumtsev, F. Ferreyrol, R. Tualle-Brouri, and P. Grangier, Preparation of non-local superpositions of quasi-classical light states, *Nature Physics* **5**, 189 (2009).
- [93] H. Jeong, A. M. Lance, N. B. Grosse, T. Symul, P. K. Lam, and T. C. Ralph, Conditional quantum-state engineering using ancillary squeezed-vacuum states, *Phys. Rev. A* **74**, 033813 (2006).
- [94] D. V. Sychev, V. A. Novikov, K. K. Pirov, C. Simon, and A. I. Lvovsky, Entanglement of macroscopically distinct states of light, *Optica* **6**, 1425 (2019).
- [95] A. P. Lund, H. Jeong, T. C. Ralph, and M. S. Kim, Conditional production of superpositions of coherent states with inefficient photon detection, *Phys. Rev. A* **70**, 020101 (2004).
- [96] A. Laghaout, J. S. Neergaard-Nielsen, I. Rigas, C. Kragh, A. Tipsmark, and U. L. Andersen, Amplification of realistic schrödinger-cat-state-like states by homodyne heralding, *Phys.*

Rev. A **87**, 043826 (2013).

- [97] A. V. Baeva, N. G. Veselkova, N. I. Masalaeva, and I. V. Sokolov, Measurement-assisted non-gaussian gate for schrödinger cat states preparation: Fock resource state versus cubic phase state, *The European Physical Journal D* **78**, 10.1140/epjd/s10053-023-00796-1 (2024).
- [98] I. Sokolov, Schrödinger cat states in continuous variable non-gaussian networks, *Physics Letters A* **384**, 126762 (2020).
- [99] F. Mehler, Ueber die entwicklung einer function von beliebig vielen variablen nach laplaceschen functionen höherer ordnung., *Journal für die reine und angewandte Mathematik* **66**, 161 (1866).
- [100] A. Erdélyi, W. Magnus, F. Oberhettinger, and F. Tricomi, *Higher Transcendental Functions* (McGraw-Hill Book Company, New York, NY, USA; Toronto, ON, Canada; London, UK, 1953).

Appendix A: Wigner Function from Mehler Formula

In this section, we describe how to calculate the Wigner function efficiently, avoiding heavy numerical integration while maintaining high accuracy. This approach is based on the technique of generating functions and is especially suited for symbolic computation environments like Maple or Mathematica to deal with power series expansions.

We apply our method to the Wigner function (19) of the exact solution given by Eqs (15), (16) and (18). To this end, the expression for the Wigner function can be conveniently rewritten in the form

$$W_n(\tilde{x}, \tilde{p}) = \frac{1}{\pi \tilde{N}_n} \int_{-\infty}^{\infty} \tilde{w}_n(\tilde{x}, z) e^{2i\tilde{p}z} dz \quad (\text{A1})$$

$$\tilde{w}_n(\tilde{x}, z) = \frac{1}{\pi^{1/2} 2^n n!} H_n(\tilde{x} - z) H_n(\tilde{x} + z) \times \exp\{-\tilde{x}^2 - (\tilde{x} + \Delta x)^2 - 2z^2\} \quad (\text{A2})$$

$$\tilde{N}_n = \int_{-\infty}^{\infty} \tilde{w}_n(\tilde{x}, 0) d\tilde{x} \quad (\text{A3})$$

where $\tilde{x} = x - y_m$, $\tilde{p} = p - p_0$ and $\Delta x = y_m - p_0$.

The well-known Mehler formula [99, 100]

$$\sum_{n=0}^{\infty} \frac{\rho^n}{2^n n!} H_n(x_1) H_n(x_2) = \frac{1}{\sqrt{1 - \rho^2}} \times \exp\left\{\frac{2\rho x_1 x_2 - \rho^2(x_1^2 + x_2^2)}{1 - \rho^2}\right\}, \quad (\text{A4})$$

can now be used to evaluate the generating functions

$$\sum_{n=0}^{\infty} \tilde{N}_n \rho^n = \frac{1}{\sqrt{2(1 - \rho)}} e^{-\frac{\Delta x^2}{2}(1 - \rho)}, \quad (\text{A5})$$

$$\sum_{n=0}^{\infty} \rho^n \int_{-\infty}^{\infty} \tilde{w}_n(\tilde{x}, z) e^{2i\tilde{p}z} dz = \frac{e^{-\Delta x^2/2}}{\sqrt{2}} W_0(\tilde{x}, \tilde{p}) \times \frac{1}{\sqrt{1 + \rho}} \exp\left\{\frac{2\rho\tilde{x}^2}{1 + \rho} + \frac{\rho\tilde{p}^2}{2}\right\}, \quad (\text{A6})$$

where

$$W_0(\tilde{x}, \tilde{p}) = \frac{1}{\pi} \exp\left\{-2(\tilde{x} + \Delta x/2)^2 - \frac{\tilde{p}^2}{2}\right\}. \quad (\text{A7})$$

The final result reads

$$W_n(\tilde{x}, \tilde{p}) = W_0(\tilde{x}, \tilde{p}) \frac{\tilde{W}_n(\tilde{x}, \tilde{p})}{N_n}, \quad (\text{A8})$$

$$\sum_{n=0}^{\infty} \tilde{W}_n(\tilde{x}, \tilde{p}) \rho^n = \frac{1}{\sqrt{1 + \rho}} \exp\left\{\frac{2\rho\tilde{x}^2}{1 + \rho} + \frac{\rho\tilde{p}^2}{2}\right\}, \quad (\text{A9})$$

$$\sum_{n=0}^{\infty} N_n \rho^n = \frac{e^{\frac{\rho\Delta x^2}{2}}}{\sqrt{1 - \rho}}. \quad (\text{A10})$$

For the photon number n , formula (A8) gives the Wigner function W_n expressed terms of the function \tilde{W}_n and the normalization coefficient N_n that can be found as coefficients of power series expansions in ρ of the corresponding generating functions. The right-hand sides of Eqs. (A9) and (A10) provide analytical expressions for these functions.